

Andean Geology ISSN: 0718-7092 ISSN: 0718-7106

andeangeology@sernageomin.cl Servicio Nacional de Geología y Minería

Chile

# Surface velocities of Upsala glacier, Southern Patagonian Andes, estimated using cross-correlation satellite imagery: 2013-2014 period

Moragues, Silvana; Lenzano, M. Gabriela; Lo Vecchio, Andrés; Falaschi, Daniel; Lenzano, Luis Surface velocities of Upsala glacier, Southern Patagonian Andes, estimated using cross-correlation satellite imagery: 2013-2014 period

Andean Geology, vol. 45, no. 1, 2018

Servicio Nacional de Geología y Minería, Chile

Available in: https://www.redalyc.org/articulo.oa?id=173954358005

DOI: https://doi.org/10.5027/andgeoV45n1-3034



Artículos de Investigación

Surface velocities of Upsala glacier, Southern Patagonian Andes, estimated using cross-correlation satellite imagery: 2013-2014 period

Silvana Moragues CONICET, Argentina smoragues@mendoza-conicet.gob.ar

DOI: https://doi.org/10.5027/andgeoV45n1-3034 Redalyc: https://www.redalyc.org/articulo.oa? id=173954358005

M. Gabriela Lenzano CONICET, Argentina mlenzano@mendoza-conicet.gob.ar

Andrés Lo Vecchio CONICET, Argentina anlovecchio@mendoza-conicet.gob.ar

Daniel Falaschi CONICET, Argentina dfalaschi@mendoza-conicet.gob.ar

Luis Lenzano CONICET, Argentina llenzano@mendoza-conicet.gob.ar

> Received: 12 January 2017 Accepted: 22 September 2017

#### ABSTRACT:

In this study we present surface velocities estimation for the Upsala glacier catchment, South Patagonian Ice Field (SPI) during the summer season of years 2013 (January-March) and 2014 (March-April), including the Bertacchi, Cono, and Murallón tributaries using satellite images from Advanced Spaceborne Thermal Emission and Reflection Radiometer (ASTER). The Cross-Correlation method was applied by COSI-Corr technique with sub-pixel accuracy. In general, it should be noted that the SPI glaciers, and Upsala glacier in particular, are fast-flowing ice bodies, which makes the technique works properly. Results of surface velocities estimation ranged from 0.22 to 2.93 md-1 for January-March 2013 and 0.12 to 5.8 md-1 for March-April 2014. In summary, COSI-Corr can achieved accurate and reliable results for glacier displacements and surface velocities estimation, also contributing in the better knowledge of the velocities change processes in time, taking into account Upsala is one of the most dynamic temperate glaciers of the SPI.

KEYWORDS: Cross-correlation, COSI-Corr, Surface velocities, ASTER, Upsala glacier.

# 1. Introduction

Glaciers worldwide stand out as one of the best climate change indicators, such as the fluctuations like a function of height (Oerlemans, 2005), and the calving glaciers are particularly sensitive due to the loss of mass in the terminus (Badino and Romeo, 2005). In recent decades, the globally widespread trend of glacier area loss has accelerated (Rignot and Kanagaratnam, 2006; Ding et al., 2006; Bolch et al., 2012; Zemp et al., 2015; Solomina et al., 2016; Yang et al., 2016; Ragettli et al., 2016) and the dynamics of glaciers has consequently readjusted (Bolch et al., 2012). In the Southern Andes, the Southern Patagonian Ice Field (SPI) constitute the largest masses of glacier ice in the Southern Hemisphere (Aniya, 2013). Glacier thinning in the SPI has sped up since 1968 (Rignot et al., 2003; Glasser et al., 2011; Willis et al., 2012), thus making an increasing



contribution to the recent sea level rise (Rignot et al., 2003). Upsala glacier, in particular, began a phase of abrupt retreat in 1978 (Naruse and Skvarca, 2000), to the present day, making it one of the most dynamic glaciers of the SPI (Sakakibara et al., 2013).

The properly assess and monitor the glaciers dynamics requires the detailed mapping of surface velocities and changes in geometry (Howat et al., 2007). In temperate glaciers, the surface velocity is defined by internal ice deformation and basal sliding, each of them affecting differently according to the time of the year (Benn and Evans, 2010). Because glaciers are generally found in remote areas of difficult access, in-situ measurements are costly and time-consuming (Herman et al., 2011). In contrast, remote sensing techniques have offered in the last decades tools for glacier monitoring thanks to the availability, of satellite imagery relying in both optical (Kääb, 2002; Berthier et al., 2005; Quincey and Glasser, 2009) and Synthetic Aperture Radar (SAR) images (Rignot and Kanagaratnam, 2006; Luckman et al., 2007), amongst others. Advances in methods and techniques for detecting changes in glaciers, such as surface velocities, have been used during the last decades. Currently, three methods are commonly employed to derive glacier-surface velocities: interferometry of SAR imagery, SAR tracking techniques, and cross correlation of optical satellite images (Scherler et al., 2008). Cross-correlation of satellite imagery has been largely utilized for mapping and monitoring glacier velocities in several mountain regions around the globe (Taylor et al., 2008; Heid and Kaab, 2011; Heid, 2011; Herman et al., 2011).

In this sense, cross-correlation technique by COSI-Corr (Co-registration of Optically Sensed Images and Correlation) software developed by Leprince et al. (2007a, b, 2008), provides robust and accurate solutions for deriving glacier surface velocities. In fact, the orthorectification of images by means of this technique is highly accurate at the sub-pixel scale (Scherler et al., 2008; Ayoub et al., 2009). In the Argentinean Andes, however, glacier velocities determinations relying on this method remain scarce, and limited to a few areas, like Monte Tronador, North Patagonian Andes (Ruiz et al., 2015) and Horcones Inferior Glacier, Mount Aconcagua, Central Andes (Pitte et al., 2016). Although in the area under study surface velocity studies have been performed with the cross-correlation technique, none of them have used COSI-Corr.

Estimation of surface velocities studies in the Upsala catchment have been carry out by different techniques, such as aerial photogrammetry (Aniya and Skvarca, 1992), topographic surveys (Naruse and Aniya, 1992; Skvarca et al., 1995) and both optical (Skvarca et al., 2003; Sakakibara et al., 2013; Sakakibara and Sugiyama, 2014; Mouginot and Rignot, 2015) and SAR satellite images (Floricioiu et al., 2008; Floricioiu et al., 2009; Muto and Furuya, 2013; Mouginot and Rignot, 2015). These studies have estimated the evolution of glacier velocities from 1968 to 2011, considering different time scales (years or decades) and using various sensors and techniques (Table 1).



TABLE 1. PREVIOUS STUDIES OF SURFACE VELOCITIES OF UPSALA GLACIER (1968-2014). THE VALUES ARE EXPRESSED IN THE UNITS AS SHOWN BY AUTHORS.

Authors (Year)	Period	Technique and images used	Surface Velocities		
Aniya and Skvarca, 1992	1968-1970 (16 months)	Arial photography and satellites images (Landsat)	675-700 my <sup>-1</sup>		
Naruse et al., 1992	November 1990	GPS	$3.5$ and $3.7$ $md^{-1}$		
Skvarca et al., 1995	November 1993	GPS	1,600 my <sup>-1</sup> (4.4 md <sup>-1</sup> )		
Skvarca et al., 2003	2000-2001 (October-March- September)	Cross-Correlationwith Landsat 7 ETM+ images.	1,679 my <sup>-1</sup> (4.41- 4.47 md <sup>-1</sup>		
Floricioui et al., 2008	2007-2008 (December-January)	Feature tracking by amplitude correlation, with Terra-SAR images.	5.6 md <sup>-1</sup>		
Floricioui et al., 2009	January 2008 October 2008 May 2009	$\label{eq:Feature tracking by amplitude correlation} Feature tracking by amplitude correlation, with Terra-SAR images.$	5.6 md <sup>-1</sup> 6.6 md <sup>-1</sup> 7.5 md <sup>-1</sup>		
Sakakibara <i>et al.,</i> 2013	2001 2002 2005 2006 2007 2008 2009	Following of surface characteristics, like crevices or seracs, with Landsat 7 ETM+ images.	1,050 my <sup>-1</sup> 1,100 my <sup>-1</sup> 1,000 my <sup>-1</sup> 1,100 my <sup>-1</sup> 1,100 my <sup>-1</sup> 1,200 my <sup>-1</sup> 1,500 my <sup>-1</sup>		
Muto and Furuya, 2013	2003-2005 2010-2011	Cross-Correlation, whit RADAR images.	2 md <sup>-1</sup> 3.5 md <sup>-1</sup>		
Sakakibara and Sugiyama, 2014	2000-2002 2004-2007 2008-2009-2010	Normalized Cross-Correlation of spatial variations in image, with Landsat TM and/or ETM+ images.	1,870-1,620 my <sup>-1</sup> 1,500-1,850 my <sup>-1</sup> 1,990-2,400-3,400 my <sup>-1</sup>		
Mouginot and Rignot, 2015	1993 1996 2001 2005 2007 2008 2010-2011 2014	Cross-Correlation, with data collected by five SAR satellites and Landsat managed by four space agencies.	0.1 km/yr 0.5 km/yr 0.8-1 km/yr 0.6 km/yr 0.9 km/yr 1.2 km/yr 1.3 km/yr 1.3 km/yr		

Table 1

The main goal of the present study is to estimate surface velocities for Upsala glacier and its tributaries Bertacchi, Cono and Murallón as well as the update of the last period studied of Upsala glacier's surface speeds to 2014, since detailed information was available until 2011. We use a temporal series of optical satellite images acquired by the Advanced Spaceborne Thermal Emission and Reflection Radiometer (ASTER) sensor (15 m resolution, www.lpdaac.usgs.gov (last visit 22-03-2016)) during the summer periods of the years 2013 (January-March) and 2014 (March-April). The cross-correlation technique with COSI-Corr software was applied for this purpose. The investigation is a continuation of our previous effort (Moragues et al., 2016). Additionally, a review of the previously published literature on surface velocities of Upsala glacier for the last seventy years, has been used for reconstructing the recent evolution of glacier velocities.



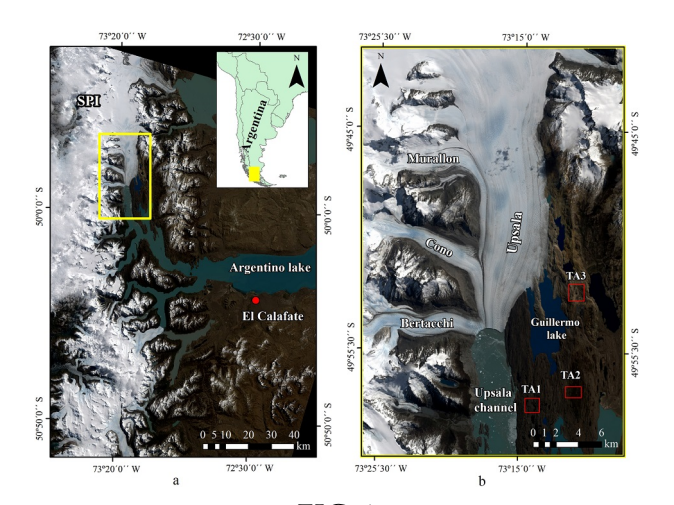


FIG. 1. a. Study area located in the Southern Patagonian Ice Field (SPI), Santa Cruz, Argentina (yellow lines); b. Upsala glacier and tributary glaciers Bertacchi, Cono and Murallón and stable test areas (red squares).

## 1.1. STUDY AREA

The study area is located at the eastern margin and latitudinally centered in the SPI (Fig. 1a), and encompasses the Upsala glacier tongue (49°50'-73°15') and its major tributaries (Bertacchi, Cono and Murallón glaciers). The main Upsala outlet glacier and the aforementioned tributaries constitute a compound basin with an area of 838 km2 (calculated from Landsat satellite images, November 2016). The main (western) glacier tongue calves into Argentino Lake and a secondary (eastern) tongue discharges in the Guillermo proglacial lake (Fig. 1b) (Skvarca, 2002).

The Holocene recession of Upsala glacier exposed Brazo Cristina more than 10,115±100 calyrs BP. The Upsala glacier readvanced at least seven times, the first being a relatively minor expansion documented only in stratigraphic sections between 7,730±50 and 7,210±45 calyrs BP (Strelin et al., 2014). The recent glacier retreat has exposed a number of proglacial features, such as striated pavements, vast moraine deposits, and rochemoutonnées, among others.

Climate in this region is characterized by the westerly flow that carries humidity from the Pacific Ocean. This system hits the area more pronouncedly during the austral winter months (July-September) (Garreaud, 2009), producing precipitation maxima of up to 10,000 mm over the Southern Patagonian Icefield (Villalba et al., 2003; Garreaud et al., 2013). Due to the strong W-E orographic precipitation gradient, precipitation over the eastern slopes of the Argentinean Andes decrease to less than 300 mm within 100 km of the main Andean axis (Villalba et al., 2003).

#### 2. Data Sets

The present study is based on four 15 m spatial resolution ASTER images (3N band) (Table 2). The ASTER images were obtained from the United States Geological Survey (USGS) Earth Explorer portal, and there were acquired during the ablation period years 2013 and 2014 (January-April), contain no significant seasonal snow, and are devoid of clouds. Note that time separation between processed scenes is crucial for the calculation of surface velocities and their uncertainties (Berthier et al., 2005), i.e., separation in days must be long enough to show the velocity signal in the slower sectors of the glacier, but short enough to preserve the morphological features that are tracked down in the correlation process.



The Shuttle Radar Topography Mission (SRTM), carrying interferometric synthetic aperture radar (SAR) sensor in C-band, acquired altitudinal data between 11 and 22 February 2000 (www.jpl.nasa.gov/srtm, (last visit 16-04-2016)). We used the SRTM DEM with processing level of 1 Arc-Second, 30 m resolution, obtained from the USGS, data pool to resolve the orthorectification processes. To provide an optimal coregistration between the ASTER imagery and the SRTM (Ayoub et al., 2015), all data was projected to the UTM zone 18S projection, and re-sampled to 30 m spatial resolution by bilinear interpolator.

In addition, Corona, Hexagon and Landsat images were used to map the historical reconstruction of the frontal positions since 1968 until 2016 (Table 2). The images were selected according to their availability in the archive. Corona and Hexagon scenes (10 m resolution) (Fowler, 2013) were geometrically treated to eliminate the produced deformations and were georeferenced through the incorporation of ground control points (GCPs) from Landsat images, and re-sampled to the same spatial resolution of Landsat (Masiokas et al., 2015). The horizontal average errors were 1.2 pixels. To more detail of the overall processing, see Hollingsworth et al. (2012). All of the process described below was done using SOPI GIS software. We use a manual delineation to detect the changes on the front positions (Nuth et al., 2013). An axial profile (A) was drawn trough the main flux of Upsala glacier to monitor the fluctuations. The origin (zero) of the axis was taken in the high zone of the central flow.

TABLE 2. SATELLITE IMAGES (INPUT DATA).

Year Sensor		Scene ID	Acquisition date mm-dd-yyyy	Time span (days)	Use	
1963	CORONA KH-4A	DS09059A045MC068	10-29-1963	-	Front fluctuation	
1979	Hexagon KH-9	DZB1215-500030L002001	03-20-1979	-	Front fluctuation	
1986	LANDSAT TM	LM52310951986014AAA03	02-18-1986	2	Front fluctuation	
1998	LANDSAT TM	LT52310951998031COA00	12-09-1998	-	Front fluctuation	
2000	LANDSAT ETM+	LE72310952000205COA00	01-28-2000	-	Front fluctuation	
2005	LANDSAT TM	LT52310952005050COA00	02-19-2005	5	Front fluctuation	
2009	LANDSAT TM	LT52310952009317COA00	11-13-2009	-	Front fluctuation	
2010	LANDSAT ETM+	LE72310952010024EDC00	01-24-2010	2	Front fluctuation	
2013	ASTER	AST_L1A_00301252013143719_0126 2013114303	01-25-2013	48	Cross correlation	
	ASTER	AST_L1A_00303142013143733_0315 2013112433	03-14-2013	•	Cross correlation	
2014	ASTER	AST_L1A_00303172014143715_0318 2014040216	03-17-2014	2	Cross correlatio	
	ASTER	AST_L1A_00304022014143734_0403 2014030825	04-02-2014	16	Cross correlation	
2015	LANDSAT OLI	LC82310952015014LGN00	01-14-2015	=	Front fluctuation	
2016	LANDSAT OLI	LC82310952016273LGN00	09-29-2016	-	Front fluctuation	

Table 2

## 3. Methods

# 3.1. ASTER IMAGES PAIR CROSS CORRELATION

In the first stage of COSI-Corr software, geometric artifacts such as topographic were removed by the images orthorectification to mitigate those influences in the final processes (Ayoub et al., 2015). Then, the image orthorectification processes were carried out selecting 30 tie-points (X,Y coordinates) over stable areas (mainly rock outcrops), areas outside the glaciers or with water, shade and snow cover. The tie points are defined either by taking points between the image and a georeferenced referenceimage (i.e., orthorectified image, shaded DEM, high resolution digitized map, etc.) (Ayoub et al., 2015). Thus, in this work tie points were taken between the reference image (January, 2013) and the shaded SRTM DEM. These tie-points are optimized by sub-pixel correlation and converted into Ground Control Points (GCPs) because manual tie



points selection leads to unavoidable mis-registrations between the orthorectified referenceimage and the orthorectified slaveimage. However, these mis-registrations can be reduced afterwards by optimizing the image with slave GCPs (Ayoub et al., 2009). Because GCPs have known ground coordinates, as they improve the georeferencing of the referenceand slave images. It can be assumed that GCPs can be located on the ASTER images with a±1 pixel accuracy (Berthier et al., 2005). Once the images were orthorectified, the scenes were spatially trimmed to the Upsala glacier area, tributary glaciers and surrounding terrain to avoid the presence of clouds and streamline the process.

In the subsequent, all of the ASTER images were co-registered to the reference2013 image. In a similar process to the previous one, 30 homologous points were selected and optimized between the reference2013 image and the three remaining ASTER scenes. This step assumes that the referenceimage georeferencing as faultless. After this, the referenceand slaveimages should be co-registered.

During this stage, the ASTER scenes were correlated to determine the offset in  $\Delta x$  and  $\Delta y$  coordinates. Once the multi-temporal images were orthorectified, the cross-correlation was performed in a region of interest (ROI) containing the glacier area and the immediate surroundings. The correlation was carried out in a two-step process. The first step estimates the image offset and in the second one, the offsets were obtained with sub-pixels accuracy (Ayoub et al., 2009), in this case less than 15 m. The horizontal displacements were calculated implementing the frequency correlator based on the Fourier method that is more sensitive to noise, and is therefore recommended for good quality optical images as those in the present study (Leprince et al., 2007; Ayoub et al., 2015). In the Fourier domain, the modulus of a white noise remains constant, and assuming that the images are degraded with some additive white noise, the phase information is then most likely to be biased in the high frequencies (Leprince et al., 2007a).

Low coherence values, caused by cloud cover or seasonal snow, may cause image de-correlation. Before extraction of ground displacements, areas with de-correlation were manually removed. An example of this can be found at Upsala glacier front in 2013 (Fig. 2c). The gaps were filled using the nearest neighbor interpolator. Nearest Neighbor interpolation finds the closest subset of input samples to a query point and applies weights to them based on proportionate areas (Sibson, 1981).

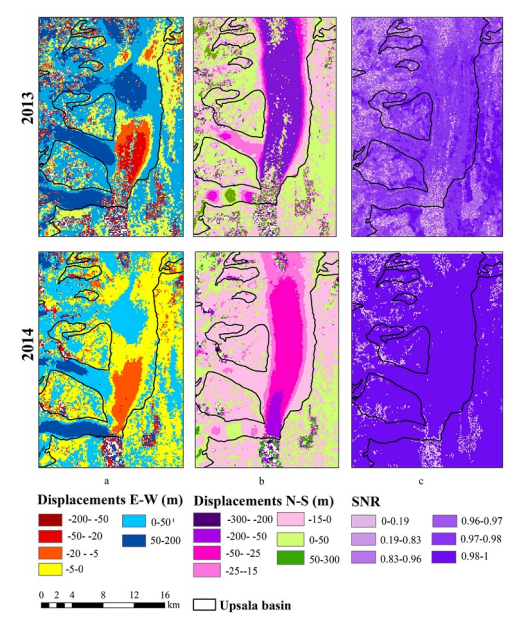


FIG. 2.

FIG. 2. Net horizontal glacier displacements for January 25 to March 14, 2013 and March 17 to April 2, 2014. Negative values indicate the direction of the N-S flow (b), while the positive values correspond to the flow W-E (a). SNR values for low correlation tend to be 0 (c). Negative N-S values indicate northerly flow (b), whereas positive W-E values correspond to Easterly flow (a). SNR values of low correlation tend to 0 (c).



#### 3.2. Extraction of glacier displacements

To obtain the values of large glacier displacements in the velocity field, multiple scale correlation analysis was performed with an initial search window size of 64 to 32 pixels, with steps of 8 pixels. The COSI-Corr cross correlation process output consists in the horizontal  $\Delta x$  (E-W) and  $\Delta y$  (N-S) displacements, and an additional SNR (Signal to Noise Ratio) one that numerically evaluates the quality of the measurement. Note that in a range of 0 to 1, a higher SNR indicates a better correlation. In some areas, the correlation is lost, then SNR reach very small atypical values close to 0 (Ayoub et al., 2009). The resultant glacier displacements are obtained by using

$$\sqrt{x^2 + y^2}$$

The daily velocity field calculation (in md-1) was obtained by dividing each of the displacement values by the number of days elapsed between the referenceand slave images (Fig. 3).

Axial and transversal profiles were identified to extract the velocities field in the Upsala, Bertacchi, Cono, and Murallón glaciers (Fig. 4). In the axial profiles drawn on the tributaries (Bertacchi glacier, AB, Cono, AC and Murallón, AM), the origin (zero) was taken from the accumulation zone to the frontal zone. In the case of Upsala (AU), the origin was taken according to the border of the selected images. The transverse ones in Upsala (TU1, TU2) were traced from the West margin to the East margin. The cross-wises in the tributaries (Bertacchi glacier, TB1, TB2, Cone, TC1, TC2 and Murallón, TM1, TM2) were drawn in two areas, one in the lower part, near the front; and the other in the upper part on changes of topography, traced from South to North. In all cases the distances were expressed in meters.

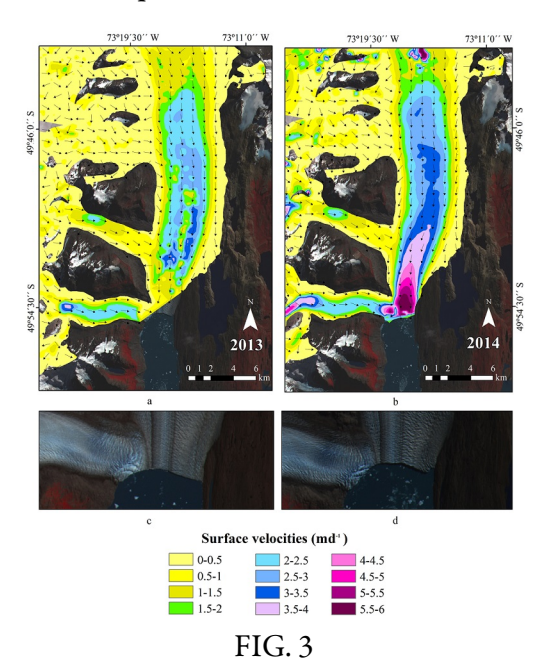


FIG. 3. Flux and ice surface velocities, expressed in meter/day, on Upsala glacier and its tributaries, derived from the cross-correlation method with ASTER images (a 2013; b 2014). (c-d) Front evolution of Bertacchi glacier in 2013 and 2014 where in 2014 (right) it shows the glacier front and its interaction with the lake. Vectors in black: velocities derived by cross-correlation.



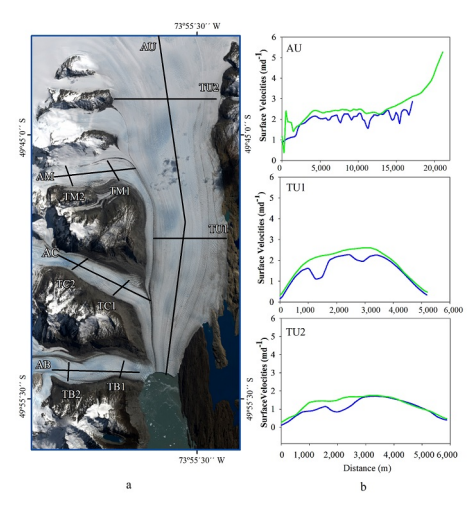


FIG. 4.

FIG. 4. a. Axial and transversal profiles were identified to extract the velocities field in the Upsala, Bertacchi, Cono, and Murallón glaciers; b. Changes in surface velocities of Upsala glacier in January-March 2013 (blue line) and March-April 2014 (green line). (AU) Axial profile, drawn from the accumulation zone to the frontal zone, distance in meters. (TU1-TU2) Transverse profile, drawn from West to East, in meters.

# 3.3. Uncertainty estimation

The cross correlation is limited to a certain degree by the surface changes due to the different illumination/incidence angles among the different satellite images (Berthier et al., 2005). This cause changes in the shadow extent and apparent displacements in shadow areas between the referenceand slave scenes, unrelated to glacier flow.

The random error ( $\sigma r$ ) was calculated on stable terrain and we choose three test areas (TA1, TA2, TA3) (Fig. 1b), where no terrain displacements is to be expected (Berthier et al., 2005; Scherler et al., 2008). Noise in displacements may resemble the Additive White Gaussian Noise. Since x and y are independent variables and follow a normal distribution. The value of the modules obeys the Rayleigh distribution and have a variance and a mean (Herman et al., 2011). For the 2013 calculation, 644 pixels were considered, whereas a total of 695 were utilized for the 2014 computation.

$$\sqrt{\Delta x^2 + \Delta y^2}$$

## 4. Results

## 4.1. GLACIER VELOCITY MAP AND PROFILES (2013-2014 PERIOD)

gure 2a and b shows the horizontal displacements in meters of the glaciers in the Upsala catchment: the Upsala glacier moves from north to south towards Argentino Lake, whereas the tributaries have displacements from west to east. The predominance of N-S displacement values in Upsala glacier ranges from 25 m to 200 m (2013-2014), with the negative sign being the N-S direction of displacement. For 2013, the maximum values of displacements, between 50 m to



Figure 2a and b shows the horizontal displacements in meters of the glaciers in the Upsala catchment: the Upsala glacier moves from north to south towards Argentino Lake, whereas the tributaries have displacements from west to east. The predominance of N-S displacement values in Upsala glacier ranges from 25 m to 200 m (2013-2014), with the negative sign being the N-S direction of displacement. For 2013, the maximum values of displacements, between 50 m to 200 m, are located in the middle of the main flow with a separation of time between images of 48 days (Fig. 2a), and for 2014 are situated near to the front (50-200 m) with a separation between scenes of 16 days (Fig. 2b). For tributary glaciers, the direction of horizontal displacement to indicate positive values in both periods, ranging from 5 m to 200 m displaced in a W-E direction. In general, in the mentioned periods, the displacements on valley glaciers have maximum values at the center of the valley, with 50 m to 200 m (W-E) for both periods. However, for the direction N-S the displacements were 50-200 m in 2013, 25-50 m in 2014, decreasing to a minimum at the margins, 0-50 m (W-E) and 0 m to 15 m (N-S) (Fig. 3a-b). Also, SNR assessing the quality of the measure shows the areas with low correlation in the terminal portion of Upsala glacier in 2013 with values between 0 and 0.2 due clouds covering (Fig. 2c).

Considering the entire Upsala basin as a whole, glacier ice presents surface velocities with a range of 0.22 to 2.93±0.06 md-1 in 2013 (Fig. 3a), and reached values of 0.12 to 5.8±0.1 md-1 in 2014 (Fig. 3b). The lower velocities correspond to the lateral margins of glaciers, whereas the maximum ones were always observed in the middle part of the Upsala glacier. The pattern of glacier direction velocities corresponds to the orientation of the ice flow (Fig. 3a-b). Thus, it can be easily noted that Upsala glacier shows an increase in velocity at a faster rate in March-April 2014 (Fig. 3b) compared to January-March 2013 (Fig. 3a). Also, the main Upsala glacier flows at higher speed than any of its tributaries. The highest velocities were recorded towards the front of Upsala glacier, coinciding with the main N-S flow direction, reaching flow rates of 2.93 md-1 in 2013, where the values can be observed in a small set of pixels of the central zone of the glacier. Due to de-correlation, the flow acceleration at the glacier front cannot be valued in figure 3a. The maximum surface velocities yielded 5.8 md-1 in 2014; the area registering these values is wider than in 2013 and represents an increase of 25% from 2013 to 2014.

The mean velocities recorded across the axial profile AU were 1.87 md-1 and 2.61 md-1 for 2013 and 2014, respectively (Table 3). In 2013, velocities across the transversal profiles of the glacier differ to a lesser degree, with a maximum of 2.3 md-1 (TU1) and 1.7 md-1 (TU2), respectively. On the other hand, in 2014, transversal TU1 and TU2 profiles also show velocity differences between the outer margin of the glacier and the middle zone, where surface velocity reached a maximum of 2.5 md-1 (TU1) and 1.8 md-1 (TU2). Figure 4b shows the axial and transversal profiles on Upsala glacier for the 2013-2014 period, blue color line corresponds to year 2013 and the green color to 2014, respectively. Note that data from the 2013 image the pixels with de-correlation were eliminated in the frontal area. The 2013 velocity variability is due to the presence of clouds on the glacier (Fig. 4b).

On average, and similarly to Upsala glacier, both the Bertacchi (1.73 md-1 and 2.33 md-1) and Cono (1.07 md-1 and 1.12 md-1) glaciers show higher speeds in 2014 compared to 2013, whereas Murallón glacier slowed down from 0.4 md-1 to 0.16 md-1 (Table 3). The second fastest glacier in the Upsala catchment was Bertacchi with maxima of 2.8 md-1 (2013) and 4.9 md-1 (2014), followed by Cono (1.6 md-1 and 1.8 md-1) and Murallón (1 md-1 and 2.2 md-1). Interestingly, despite the fact that axial profiles show increased velocities in 2014, the transversal profiles AB, AC and AM at the tributary glaciers terminus show only minor variability in flow rates. On the contrary, increases in glacier velocity in these tributaries have concentrated in the upper portions of the ablation areas.



TABLE 3. MEAN SURFACE VELOCITIES BY PROFILE ON GLACIERS IN THIS STUDY.

Glacier	Axial (md <sup>-1</sup> )		Transverse (md <sup>-1</sup> )					
	2013 20		Low		Medium		High	
		2014	014 2013	2014	2013	2014	2013	2014
Upsala (AU, TU1, TU2)	1.87	2.62	-	-	1.57	1.87	1.10	1.28
Bertacchi (AB, TB1, TB2)	1.73	2.33	1.41	1.39	-	(2)	1.09	1.60
Cono (AC, TC1, TC2)	1.07	1.12	0.64	0.59	-	-	1.17	1.44
Murallón (AM, TM1, TM2)	0.40	0.16	0.31	0.30	-	-	0.17	0.89

Table 3

#### 5. Discussion

Image quality is one of the factors limiting the accuracy of glacier surface speed estimation in a multitemporal analysis of satellite images. Satellite based optical sensors may often have observation limiting factors, such as cloud cover, especially in mountain regions (Gleitsmann and Kappas, 2006) such as in the SPI region. In this sense, the 2013 ASTER pair, used in this study, had severe issues with areas of image de-correlation compared to the 2014 pair. We associated the low correlation areas with the presence of variable seasonal snow, clouds and changing illumination conditions between the images. Although this situation, it was possible to estimate accurate results of surface speed motion for the Upsala glacier in the 2013-2014 period.

### 5.1. Surface velocities of Upsala Glacier

Considering the mean surface velocities at the glacier terminus found in the present study of Upsala catchment (2013-2014), maximum velocities correspond to the main Upsala glacier (2.93 and 5.8 md-1) followed by Bertacchi (2.8 and 4.9 md-1), Cono (1.6 and 1.8md-1) and lastly Murallón (1 and 2.2 md-1), for the years 2013 and 2014, respectively. We further calculated the uncertainty in glacier velocity at 0.06 md-1 (2013) and 0.10 md-1 (2014).

As shown in table 1, the lowest surface velocities known for the Upsala glacier were estimated by Aniya and Skvarca (1992), between 1968 and 1970, with a velocity of 700 my-1 (1.9 md-1). Mouginot and Rignot (2015) presented a comprehensive study of Upsala glacier surface velocities in the NPI and SPI between 1993 and 2014, revealing a velocities increase between 1993 (0.30 md-1) and 2001 (2.75 md-1), but later decreased by 20% between 2001 and 2005. In the same study authors report that between 2005 and 2010, the glacier sped up yet again by 50% before decreasing again in 2014 (3.56 md-1). In addition, Sakakibara and Sugiyama (2014) found velocities higher than 3,000 my1 (8.22 md1) near the calving front for 2010 year, when most freshwater glaciers in the SPI had a general deceleration trend.

The acceleration of surface velocities found in the period 2013-2014 has been related to the calving processes and the interaction between the glacier itself and the Argentino Lake (Sugiyama et al., 2016). On calving glaciers, surface velocities reach a maximum at the glacier front, due to the pulling effect of high calving rates (Sakakibara and Sugiyama, 2014). Upsala glacier has been in fact described as one of the most representative glaciers in this regard (Sakakibara et al., 2013). The high calving rates may be further enhanced when near-buoyancy conditions are reached at the front of a glacier calving into deep waters (Rivera et al., 2012). In the case of Upsala, this is confirmed by the recently bathimetric survey of the lake, where in 2016 it was investigated until approximately 600 m near the front of the glacier (Sugiyama et al., 2016). The glacier



retreat and surface velocity of large calving glaciers of the SPI are driven by the bedrock topography (Naruse and Skvarca, 2000; Skvarca et al., 2002), which in turn is related to lithology (Kraemer and Riccardi, 1997), and may be unrelated to the climate variability to a great extent (Yde and Paasche, 2010; Post et al., 2011; Wilson et al., 2016). The great depth of the Argentino Lake and the Upsala channel in particular might be related to the abundance of easily erodible rocks such as the slates of Pizarras Formation in the Upsala basin (Lo Vecchio et al., 2016). This noticeable acceleration of glaciers at their terminus has been previously described for other outlet glaciers in Patagonia such as Jorge Montt (Rivera et al., 2012; Sakakibara and Sugiyama, 2014; Bown, 2015), where calving is driven at least in part by water depths near the front.

## 5.2. Frontal position and surface velocities variation

ak

Sakakibara and Sugiyama (2014) studied the glacier frontal variations of the outlet glaciers in the SPI. These authors reported a general recession trend for most glaciers in the area, though spatially and temporally varied. The ice speed acceleration implied a substantial increase in frontal ablation (calving plus subaqueous frontal melting) (Sugiyama et al., 2016). This statistically consistent and significant recession suggests the existence of warming trend in the region. However, there is not yet enough statistical evidence of climate data within the ice field to state that a regional atmospheric warming is the cause of glacier retreat (Skvarca and De Angelis, 2002).

We examined the relationship between the frontal positions and variations of the surface speeds of the Upsala glacier (Fig. 5). For this figure, we took into consideration the different techniques and acquisition dates for each of the studies listed in table 1. To make the comparison easy, we refer to the glacier surface velocities as near as possible to the glacier terminus (e.g., Sakakibara et al., 2013; Muto and Furuya, 2013), and the original my-1 values were converted into md-1 rates. We detected at least two episodes where a surface velocity increase coincided with enhanced glacier retreat. The first one is observed for the 1993-2002 period, when the glacier reached velocities up to 4.4 md-1 in the year 1993 (Skvarca et al., 1995), whereas between 2000 and 2002 maximum velocities exceeded 4.7 md-1 (Sakakibara and Sugiyama, 2014). The surface velocity of Upsala glacier increased significantly starting in the year 2008, coinciding with the rapid retreat of the frontal position. This velocity increase (2000-2008) coincides with an enhanced -90 my-1 retreat rate. On the other hand, during the 2009-2010 period, Sakakibara and Sugiyama (2014) reported a maximum glacier velocity of 9.3 md-1 (historical maximum registered so far for Upsala glacier), coinciding with an abrupt retreat rate of 1,000 my-1 approx.

Figure 5b shows a rough estimate of Upsala glacier terminus positions from early 20th century based on Warren et al.(1995) (1914-1945 period), and additional mapping on CORONA (1963-1979) and Landsat imagery (1985-2016). At least three stages of varied retreat rates can be recognized. During the first stage (1914-1945), Upsala glacier retreated at -193 my-1. In the second stage (1940-1978), the glacier was fairly stable, retreating merely 30 my-1. Throughout this second phase, Upsala glacier occupied the shallower part of the Upsala channel south of the Vacas valley, (Skvarca et al., 2002), where extensive rock exists. The combination of these two factors may have contributed to the stabilization of the glacier front during this period. After this relatively stable period, the glacier terminus begun a steady and fast retreat phase in 1978 (Naruse and Skvarca, 2000) that is presently ongoing, and which represented approximately 15% of the total mass loss of the ice field between February 2000 and August 2011 (Willis et al., 2012). This stage is characterized by retreat rates of -263 my-1, which are in agreement with those found for Jorge Montt glacier (-240 my-1) for the 2000-2012 period (Sakakibara and Sugiyama, 2014). In terms of glacier elevation changes, Willis et al. (2012) determined thinning rates of 24 my-1 at the glacier snout for the 2000-2012 period. Mean rates of frontal recoil of 400 my-1 (Skvarca et al., 2003), with estimated maxima higher than 800 my-1 (Naruse et al., 1997) make Upsala one of the most dynamic glaciers of SPI.



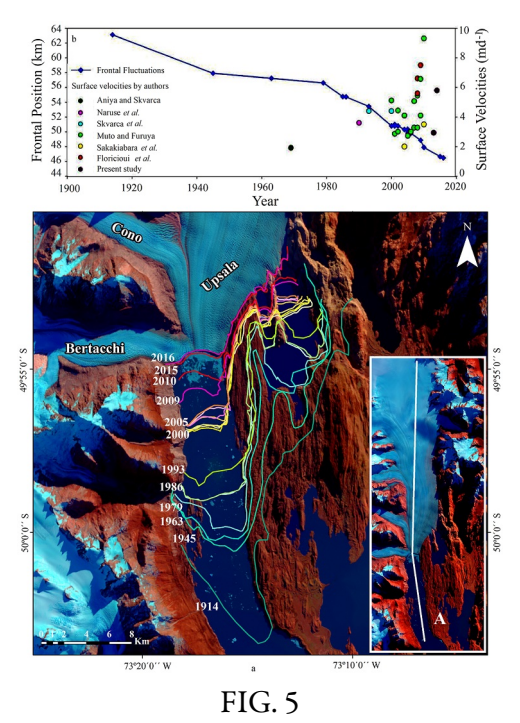


FIG. 5. a. Temporal evolution of Upsala glacier frontal position, from 1914 to 2016 and the registration of studies carried out by different authors from the end of the 20th century to the present day on the surface velocities of the frontal area or the nearest sector recorded, expressed in md-1 (upper); b. Front fluctuations of Upsala glacier since 1914 at present (lower), the profile (A) by which the glacier retreated was calculated in kilometers, from the accumulation zone towards the frontal zone.

#### 5.3. Bertacchi glacier retreat

Due to the fast retreat of Upsala glacier, the tributary Bertacchi tongue is no longer restrained at its terminus (Fig. 6). Thus, the glacier may be subject to longitudinal stress due to a new, faster flow rate, and this longitudinal stretching may lead to increased velocities in certain glacier areas. Since glacier movement responds to the viscous-elastic flow laws and flows in response to gravity, the glacier areas with steeper slopes should be the most affected by this process (Fig. 6). Higher glacier velocities (4 md-1 in the upper ablation area and 5.5 md-1 at the terminus) coinciding with abrupt slope areas can be observed in figure 6. Presently, the terminus of Bertacchi glacier is now calving into Argentino Lake and may be undergoing similar glacier-lake interactions as in the large outlet glaciers (Fig. 3d).



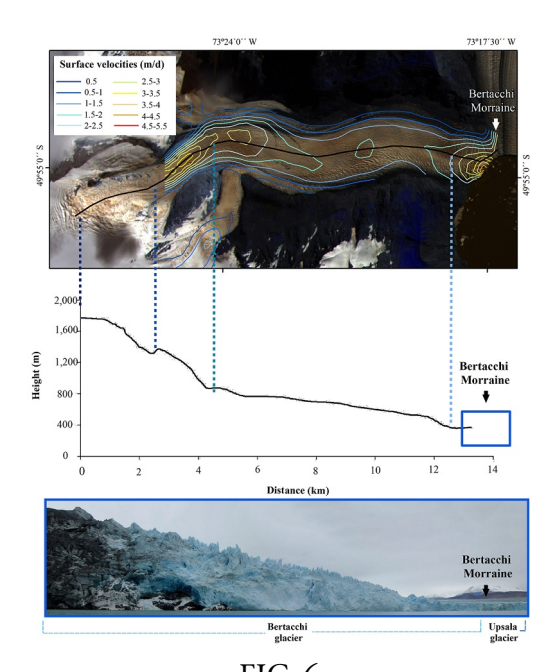


FIG. 6. lacier in the year 2014, expressed in

FIG. 6. Isolines surface velocities of the Bertacchi Glacier in the year 2014, expressed in md-1 (upper). Topographic profile of the bed rock glacier (black line), dotted lines delimit the areas with steeper slopes (average). Panoramic photograph of the front of Bertacchi glacier, in contact with the vertical front of the Upsala glacier to the right (lower).

#### 6. Conclusions

Upsala glacier is one of the temperate glaciers of high scientific interest in the SPI as it presents a combination of processes and mechanisms such as rapid frontal retreating, surface velocity variations, ablation and mass balance changes, high calving rates, thinning dynamic features, that make it a highly active glacier. From the late 20th century to the present, it had a high rate of frontal retraction and an acceleration of exceptional surface velocities, compared to other glaciers studies in the SPI.

The present study estimates surface velocities of Upsala glacier and tributary glaciers, by means of cross-correlation of ASTER images with the COSI-Corr software. The technique proved to be appropriate for the detection and estimation of glacier displacements and velocities, as it offered an operative sub-pixel methodology for the measurements of the horizontal flow, taking in consideration a fast-flowing glacier such as Upsala. In addition, the investigation makes a significant contribution to the understanding of the dynamic of Upsala glacier, since it adds new data to the previously published studies focusing on glacier velocity, extending the surveyed period until 2014. Results of surface velocities estimations ranged from 0.22 to 2.93 md-1 for january-march 2013 and 0.12 to 5.8 md-1 for march-april 2014. The available glacier velocities were put into context of glacier fluctuations since 1914 and a tight correspondence between glacier velocities and retreat rates was implied.

#### ACKNOWLEDGEMENTS

This work has been funded by the Agencia Nacional de Ciencia y Tecnología of Argentina (grants PICT 2921-2012 and PICT 1995-2013). The authors thank C. Cagliari, R. Bruce, E. Lannutti for their collaboration and relevant contributions during the preparation of the manuscript.



## REFERENCES

- Aniya, M. 2013. Holocene glaciations of Hielo Patagónico (Patagonia Icefield), South America: A brief review. Geochemical Journal 47 (2): 97-105.
- Aniya, M.; Skvarca, P. 1992. Characteristic and variations of Upsala and Moreno glaciers, Southern Patagonia. Bulletin of Glacier Research 10: 39-54.
- ASTER imagery. 2013-2014. SRTM DEM downloaded from the USGS through the Earth Explorer data poll at http://www.earthexplorer.usgs.gov (las visit 12/01/2017).
- Ayoub, F.; Leprince, S.; Avovac, J.P. 2009. Co-registration and correlation of aerial photographs for ground deformation measurements. ISPRS Journal of Photogrammetry and Remote Sensing 64: 551-560.
- Ayoub, F.; Leprince, S.; Avouac, J.P. 2015. User's Guide to COSI-CORR Co-registration of Optically Sensed Images and Correlation. California Institute of Technology 1200 East California Blvd, Pasadena, CA 91125, USA: 1-48.
- Badino, G.; Romeo, A. 2005. Crio-Karst in the Hielo Continental Sur. Glacier Caves and Glacial Karst in High Mountains and Polar Regions (Mavlyudov, B.R.; editor). Institute of Geography of the Russian Academy of Sciences: 13-18. Moscow.
- Benn, D.I.; Evans, D.J.A. 2010. Glaciers and glaciation. 2nd edition. Hodder Education: 802 p. London.
- Berthier, E.; Vadon, H.; Baratoux, D.; Arnaud, Y.; Vincent, C.; Feigl, K.L.; Rémy, F.; Legrésy, B. 2005. Surface motion of mountain glaciers derived from satellite optical imagery. Remote Sensing of Environment 95 (1): 14-28.
- Bolch, T.; Kulkarni, A.; Kääb, A.; Huggel, C.; Paul, F.; Cogley, J.G.; Frey, H.; Kargel, J.S.; Fujita, K.; Scheel, M.; Bajracharya, S.; Stoffel, M. 2012. The state and fate of Himalayan glaciers. Science 336 (6079): 310-314.
- Bown, F. 2015. Dinámica frontal de un glaciar de descarga oceánica: Glaciar Jorge Montt, Campo de Hielo Patagónico Sur. Ms. Thesis (Inédito). Universidad de Concepción: 104 p.
- Ding, Y.; Liu, S.; Li, J.; Shangguan, D. 2006. The retreat of glaciers in response to recent climate warming in western China. Annals of Glaciology 43 (1): 97-105.
- Floricioiu, D.; Eineder, M.; Rott, H.; Nagler, T. 2008. Velocities of major outlet glaciers of the Patagonia icefield observed by Terra SAR-X. IEEE International Geoscience and Remote Sensing Symposium (IGARSS): 347-350. Boston.
- Floricioiu, D.; Eineder, M.; Rott, H.; Yague-Martínez, N.; Nagler, T. 2009. Surface velocity and variations of outlet glaciers of the Patagonia Icefields by means of Terra SAR-X. In Proceedings of International Geoscience and Remote Sensing Symposium: 1028-1031. Cape Town, South Africa.
- Fowler, M.J.F. 2013. Declassified Intelligence Satellite Photographs. In Archaeology from historical aerial and satellite archives (Hanson, W.S.; Oltean, I.A.; editors). Springer Science, Business Media: 47-66. Berlin.
- Garreaud, R.D. 2009. The Andes climate and weather. Advances in Geosciences 7: 1-9.
- Garreaud, R.; López, P.; Minvielle, M.; Rojas, M. 2013. Large scale control on the Patagonia climate. Journal of Climate 26: 215-230.
- Glasser, N.F.; Harrison, S.; Jansson, K.; Anderson, K.; Cowley, A. 2011. Global sea-level contribution from the Patagonian Icefields since the Little Ice Age maximum. Nature Geoscience 4: 303-307.
- Gleitsmann, L.; Kappas, M. 2006. Glacier monitoring survey flights below clouds in Alaska: oblique aerial photography utilizing digital multiple image photogrammetry to cope with adverse weather. EAR Sele Proceedings 5 (1): 42-50.
- Heid, T. 2011. Deriving glacier surface velocities from repeat optical images. Doctoral dissertation. Ph. D. Thesis (Unpublished), University of Oslo: 120 p.
- Heid, T.; Kääb, A. 2011. Evaluation of different existing image matching methods for deriving glacier surface displacements globally from optical satellite images. Remote Sensing of Environment 18: 339-355.
- Herman, F.; Anderson, B.; Leprince, S. 2011. Mountain glacier velocity variation during a retreat/advance cycle quantified using sub-pixel analysis of ASTER images. Journal of Glaciology 57 (202): 197-207.



- Hollingsworth, J.; Leprince, S.; Ayoub, F.; Avouac, J.P. 2012. Deformation during the 1975-1984 Krafla rifting crisis, NE Iceland, measured from historical optical imagery. Journal of Geophysical Research: Solid Earth 117 (B11): B11407.
- Howat, I.M.; Joughin, I.; Scambos, T.A. 2007. Rapid changes in ice discharge from Greenland outlet glaciers. Science 315 (5818): 1559-1561.
- Kääb, A. 2002. Monitoring high-mountain terrain deformation from repeatedair-and space borne optical data: examples using digital aerial imagery and ASTER data. ISPRS Journal of Photogrammetry and Remote Sensing 57 (1-2): 39-52.
- Kraemer, P.E.; Riccardi, A.C. 1997. Estratigrafía de la región comprendida entre los lagos Argentino y Viedma (49°40'-50°10' lat. S), Provincia de Santa Cruz. Revista de la Asociación Geológica Argentina 52 (3): 333-360.
- Leprince, S.; Barbot, S.; Ayoub, F.; Avouac, J.P. 2007a. Automatic and precise ortho-rectification, co-registration and sub-pixel correlation of satellite images, application to ground deformation measurements. IEEE Transactions on Geosciences and Remote Sensing 45: 1529-1558.
- Leprince, S.; Ayoub, F.; Klinger, Y.; Avouac, J.P. 2007b. Co-registration of optically sensed images and correlation (COSI-Corr): an operational methodology for ground deformation measurements. In Proceedings of the International Geoscience and Remote Sensing Symposium: 23-28. Barcelona.
- Leprince, S.; Berthier, E.; Ayoub, F.; Delacourt, C.; Avouac, J.-P. 2008. Monitoring earth surface dynamics with optical imagery. EOS, Transactions American Geophysical Union 89 (1): 1-2.
- Lo Vecchio, A.; Lenzano, M.G.; Richiano, S.; Lenzano, L.E. 2016. Identificación y caracterización litológica mediante el uso del sensor ETM+ (Landsat 7). Caso de estudio: entorno del glaciar Upsala, Argentina.Revista de la Asociación Española de Teledetección 46: 57-72.
- Luckman, A.; Quincey, D.J.; Bevan, S. 2007. The potential of satellite radar interferometry and feature tracking for monitoring flow rates of Himalayan glaciers. Remote Sensing of Environment 111 (2-3): 172-181.
- Masiokas, M.H.; Delgado, S.; Pitte, P.; Berthier, E.; Villalba, R.; Skvarca, P.; Marinsek, S. 2015. Inventory and recent changes of small glaciers on the northeast margin of the Southern Patagonia Icefield, Argentina. Journal of Glaciology 61 (227): 511-523.
- Moragues, S.; Lenzano, M.G.; Lo Vecchio, A.; Lenzano, L.; Moreiras, S.M. 2016. Estimación de velocidades superficiales en glaciares de la zona del Parque Nacional Los Glaciares, Santa Cruz, Argentina. In Simposio Internacional Selper, No. 17: p. 325. Puerto Iguazú.
- Mouginot, J.; Rignot, E. 2015. Ice motion of the Patagonian Icefield of Soth America: 1984-2014. Geophysical Research Letters 42: 1-8.
- Muto, M.; Furuya, M. 2013. Surface Velocities and Ice-Front Positions of Eight Major Glaciers in the Southern Patagonian Ice Field, South America, from 2002 to 2011. Remote Sensing and Environment 139: 50-59.
- Naruse, R.; Aniya, M. 1992. Outline of Glacier Research Proyecting Patagonia, 1990. Bulleting of Glacier Research 10: 31-38.
- Naruse, R.; Skvarca, P. 2000. Dynamic Features of Thinning and Retreating Glaciar Upsala, a Lacustrine Calving Glacier in Southern Patagonia. Arctic, Antarctic, and Alpine Research 32 (4): 485-491.
- Naruse, R.; Skvarca, P.; Takeuchi, Y. 1997. Thinning and retreat of Glaciar Upsala, and an estimate of annual ablation changes in southern Patagonia. Annals of Glaciology 24: 38-42.
- Nuth, C.; Kohler, J.; König, M.; Deschwanden, A.V.; Hagen, J.O.M.; Kääb, A.; Pettersson, R. 2013. Decadal changes from a multi-temporal glacier inventory of Svalbard. The Cryosphere 7 (5): 1603-1621.
- Oerlemans, J. 2005. Extracting a climate signal from 169 glacier records. Science 308: 675-677.
- Pitte, P.; Berthier, E.; Masiokas, M.H.; Cabot, V.; Ruiz, L.; Ferri Hidalgo, L.; Gargantini, H.; Zalazar, L. 2016. Geometric evolution of the Horcones Inferior Glacier (Mount Aconcagua, Central Andes) during the 2002-2006 surge. Journal of Geophysical Research 121: 111-127.
- Post, A.; O'Neel, S.; Motyka, R. J.; Streveler, G. 2011. A complex relationship between calving glaciers and climate. EOS, Transactions American Geophysical Union 92 (37): 305-306.



- Quincey, D.J.; Glasser, N.F. 2009. Morphological and ice dynamical changes on the Tasman Glacier, New Zealand 1990-2007. Global Planetary Change 68 (3): 185-197.
- Ragettli, S.; Bolch, T.; Pellicciotti, F. 2016. Heterogeneous glacier thinning patterns over the last 40 years in Langtang Himal. The Cryosphere 10: 2075-2097.
- Rignot, E.; Kanagaratnam, P. 2006. Changes in the velocity structure of the Greenland Ice Sheet. Science 311 (5673): 986-990.
- Rignot, E.; Rivera, A.; Casassa, G. 2003. Contribution of the Patagonian icefields of South America to sea level rise. Science 302 (5644): 434-437.
- Rivera, A.; Corripio, J.; Bravo, C.; Cisternas, S. 2012. Glaciar Jorge Montt (Chilean Patagonia) dynamics derived from photos obtained by fixed cameras and satellite image feature tracking. Annals of Glaciology 53 (60): 147-155.
- Ruiz, L.; Berthier, E.; Masiokas, M.; Pitte, P.; Villalba, R. 2015. First surface velocity maps for glaciers of Monte Tronador, North Patagonian Andes, derived from sequential Pléiades satellite images. Journal of Glaciology 61 (229): 908-921.
- Sakakibara, D.; Sugiyama, S. 2014. ICE front variations and speed changes of calving glaciers in the Southern Patagonia Icefield from 1984 to 2011. Journal of Geophysical Research: earth surface 119 (11): 2541-2554.
- Sakakibara, D.; Sugiyama, S.; Sawagaki, T.; Marinsek, S.; Skvarka, P. 2013. Rapid retreat, acceleration and thinning of Glaciar Upsala, Southern Patagonia Icefield, initiated in 2008. Annals of Glaciology 54 (63): 131-138.
- Scherler, D.; Leprince, S.; Strecker, M.R. 2008. Glacier-surface velocities in alpine terrain from optical satellite imagery: accuracy improvement and quality assessment. Remote Sensing of Environment 112 (10): 3806-3819.
- Sibson, R. 1981. A brief description of natural neighbor interpolation. Interpreting multivariate data: 21-36.
- Skvarca, P. 2002. Importancia de los glaciares del hielo Patagónico Sur para el desarrollo regional. In Congreso Geológico Argentino, No. 15, Geología y Recursos Naturales de Santa Cruz. Instituto Antártico Argentino 1: 1-14. El Calafate. Santa Cruz.
- Skvarca, P.; De Angelis, H. 2002. Fifteen year changes of Southern Patagonia Icefield glaciers, Argentina-Chile, detected from Landsat TM mosaics. In Proceedings of the International Symposium on Remote Sensing of Environment, No. 29: 8-12. Buenos Aires.
- Skvarca, P.; Satow, K.; Naruse, R.; Leiva, J. 1995. Recent thinning, retreat and flow of Upsala Glacier, Patagonia. Bulletin of Glacier Research 13: 11-20.
- Skvarca, P.; De Angelis, H.; Naruse, R.; Warren, C.R.; Aniya, M. 2002. Calving rates in fresh water: New data from southern Patagonia. Annals of Glaciology 34: 379-384.
- Skvarca, P.; Raup, B.; De Angelis, H. 2003. Recent behaviour of Glaciar Upsala, a fast-flowing calving glacier in Lago Argentino, southern Patagonia. Annals of Glaciology 36: 184-188.
- Solomina, O.N.; Bradley, R.S.; Jomelli, V.; Geirsdottir, A.; Kaufman, D.S.; Koch, J.; Nicolussi, K. 2016. Glacier fluctuations during the past 2000 years. Quaternary Science Reviews 149: 61-90.
- Strelin, J.; Kaplan, M.; Vandergoes, M.; Denton, G.; Schaefer, J. 2014. Holocene glacier history of the Lago Argentino basin, Southern Patagonian Icefield. Quaternary Science Reviews 101: 124-145.
- Sugiyama, S.; Minowa, M.; Sakakibara D.; Skvarca, P.; Sawagaki, T.; Ohashi, Y.; Naito, N.; Chikita K. 2016. Thermal structure of proglacial lakes in Patagonia, Journal of Geophysical Research: Earth Surface 121: 2270-2286.
- Taylor, M.; Leprince, S.; Avouac, J.P.; Sieh, K. 2008. Detecting co-seismic displacements in glaciated regions: An example from the great November 2002 Denail earthquake using SPOT horizontal offsets. Earth and Planetary Science Letters 220: 209-220.
- Villalba, R.; Lara, A.; Boninsegna, J.A.; Masiokas, M.; Delgado, S.; Aravena, J.C.; Roig, F.A.; Schmelter, A.; Wolodarsky, A.; Ripalta, A. 2003. Large-scale temperature changes across the Southern Andes: 20th century variations in the context of the past 400 years. Climatic Change 59: 177-232.
- Warren, C.; Greene, D.; Glasser, N. 1995. Glaciar Upsala, Patagonia: rapid calving retreat in fresh water. Annals of Glaciology 21: 1-6.



- Willis, M.; Melkonian, A.K.; Pritchard, M.E.; Rivera, A. 2012. Ice loss from the Southern Patagonian Ice Field, South America, between 2000 and 2012. Geophysical Research Letters 39: 1-6.
- Wilson, R.; Carrión, D.; Rivera, A. 2016. Detailed dynamic, geometric and supraglacial moraine data for Glaciar Pio XI, the only surge-type glacier of the Southern Patagonia Icefield. Annals of Glaciology 57 (73): 119-130.
- Yang, W.; Guo, X.; Yao, T.; Zhu, M.; Wang, Y. 2016. Recent accelerating mass loss of southeast Tibetan glaciers and the relationship with changes in macroscale atmospheric circulations. Climate Dynamics 47 (3-4): 805-815.
- Yde, J.C.; Paasche, Ø. 2010. Reconstructing climate change: not all glaciers suitable. EOS, Transactions American Geophysical Union, AGU 91 (21): 189-190.
- Zemp, M.; Frey, H.; Gärtner-Roer, I.; Nussbaumer, S.U.; Hoelzle, M.; Paul, F.; Haeberli, W.; Denzinger, F.; Ahlstrom, A.P.; Anderson, B.; Balracharya, S.; Baroni, C.; Braun, L.N.; Cáceres, B.E.; Casassa, G.; Cobos, G.; Dávila, L.R.; Delgado Granados, H.; Demuth, M.N.; Espizua, L.; Fischer, A.; Fujita, K.; Gadek, B.; Ghazanfar, A.; Hagen, J.O.; Holmlund, P.; Karimi, N.; Li, Z.; Pelto, M.; Pitte, P.; Popovnin, V.V.; Portocarrero, C.A.; Prinz, R.; Sangewar, C.V.; Severskiy, I.; Sigurdsson, O.; Soruco, A.; Usubaliev, R.; Vincent, C. 2015. Historically unprecedented global glacier decline in the early 21st century. Journal of Glaciology 61 (228): 745-761.

